Available online at www.sciencedirect.com
SCIENCE DIRECT®
Experimental Thermal and Fluid Science 29 (2005) 773–782
Experimental Thermal and Fluid Science
www.elsevier.com/locate/etfs

Heater size and heater aspect ratio effects on subcooled pool boiling heat transfer in low-g

Christopher D. Henry [a], Jungho Kim [a,*], Brian Chamberlain [a], Thomas G. Hartman [b]

[a] Department of Mechanical Engineering, University of Maryland, College Park, MD 20742, USA
[b] Department of Food Science, Rutgers University, New Brunswick, NJ 08901-8520, USA

Abstract

Pool boiling heat transfer measurements using heaters of varying aspect ratio were obtained in low-g (0.01 g ± 0.025 g) aboard the KC-135 aircraft. The heater aspect ratio was varied by selectively powering 2×2, 2×4, 2×6, 2×8, and 2×10 arrays of heaters in a 10×10 heater array containing individual heaters 0.7×0.7 mm^2 in size. Electronic control circuitry was used to maintain an isothermal boundary condition on the heater surface while the power dissipated by the heater was measured. The working fluid was FC-72 at 101 kPa and three different bulk subcoolings. Low-g boiling behavior was governed by the dynamics of the primary bubble. For both square and rectangular heaters, CHF appeared to be a result of the competition between increasing heat transfer associated with the satellite bubbles and the decrease in heat transfer due to growth of the dry area under the primary bubble as the wall superheat increases. At low subcooling on rectangular heaters, surface tension acted to pull the bubble into a spherical shape, allowing liquid to rewet the surface. At high subcooling and high superheat, thermocapillary convection caused the large bubbles that formed on the surface to shrink by increasing the condensation on the bubble cap, resulting in more wetted area. The presence of thermocapillary convection at higher subcooolings may be due to FC-72 being a mixture of various components.

1. Introduction

An understanding of boiling and critical heat flux (CHF) in low gravity environments is of importance to the design of space based hardware and processes such as heat exchangers, cryogenic fuel storage and transportation, electronic cooling, and material processing. Lack of understanding of the effects of reduced gravity on boiling has been identified as one of the primary obstacles to implementation of high efficiency Rankine cycle based power conversion systems that are being considered for deep space and manned mission-to-Mars systems as well as for life support systems [1]. Although boiling research has been performed over the past four decades, the mechanisms by which heat is removed from heated surfaces in low gravity are still unclear. The reader is referred to [2–4] for reviews of recent reduced gravity research in Europe, the US, and Japan.

1.1. Effect of subcooling

An increase in subcooling is believed to provide higher heat transfer rates during the rewetting process. Previous investigations have shown that an increase in subcooling decreases the bubble size and causes departing bubbles to rapidly collapse [5]. Further investigations showed that subcooling had little to no effect on heat transfer during nucleate boiling in earth gravity [6]. Subcooling effects on bubble departure frequency, liquid rewetting temperature, and active site population density act to mitigate heat transfer differences compared to near saturated bulk conditions.

* Corresponding author.
E-mail addresses: cdh@wam.umd.edu (C.D. Henry), kimjh@umd.edu (J. Kim), chamberb@wam.umd.edu (B. Chamberlain), hartmantg@aol.com (T.G. Hartman).

0894-1777/$ - see front matter © 2005 Elsevier Inc. All rights reserved.
doi:10.1016/j.expthermflusci.2005.03.003

Nomenclature

A_i	area of individual heater element [m^2]
A_w	area of heated surface [m^2]
a_l	thermal diffusivity [m^2/s]
BP	Boiling point (101 kPa) [°C]
c	concentration [ppm]
c_p	specific heat of liquid [J/kg K]
C_g	Dissolved gas concentration [ppm]
C_0	0.1 (Eq. (1))
g	gravitational constant [m/s^2]
H	Henry's constant [mole/mole Pa]
h_{fg}	heat of vaporization [J/kg]
L	Marangoni length [m]
MW	molecular weight [kg/mol]
$M_{a,l}$	mass of air in liquid [kg]
n	0.75 (Eq. (1))
P_g	partial pressure of gas [kPa]
$P_{a,i}$	initial partial pressure of gas [kPa]
P_T	total pressure [kPa]
$q_{CHF,sub}$	critical heat flux, subcooled bulk conditions [W/m^2]
$q_{CHF,sat}$	critical heat flux, saturated bulk conditions [W/m^2]
ρ_l	liquid density [kg/m^3]
ρ_v	vapor density [kg/m^3]
R_a	gas constant [J/kg K]
σ	surface tension [N/m]
t	tangential coordinate direction along bubble interface
T	temperature [°C]
T_{bulk}	bulk liquid temperature [°C]
T_h	heater temperature [°C]
ΔT_{sub}	bulk liquid subcooling = $T_{sat} - T_{bulk}$ [°C]
ΔT_{sat}	wall superheat = $T_w - T_{sat}$ [°C]
T_{sat}	saturation temperature [°C]
V	volume [m^3]
V_g	volume of gas/vapor [m^3]
V_l	volume of liquid [m^3]
φ	electrical potential [V]
η	viscosity [Pa s]

Although negligible subcooling effects have been observed during nucleate pool boiling, bulk subcooling appears to significantly increase CHF by condensing vapor generated at the heated surface thereby providing less resistance for bulk liquid to rewet the surface. Kutateladze [7] postulated that CHF in subcooled boiling should increase above similar saturated conditions by the amount of energy required to bring the subcooled liquid to a saturated state:

$$\frac{q_{CHF,sub}}{q_{CHF,sat}} = 1 + C_0\left(\frac{\rho_l}{\rho_v}\right)^n \frac{c_p(T_{sat} - T_{bulk})}{h_{fg}} \quad (1)$$

Ivey and Morris [8] suggested $C_0 = 0.1$ and $n = 0.75$ based on available data.

For nucleate boiling on flat horizontal heaters in low-g, the formation of a primary bubble that causes significant dryout over the heater surface has been documented [9–11]. At low heat flux, some researchers measured a higher heat transfer compared to similar 1-g conditions [9]. Under such conditions, bubble departure can be non-existent and bubble dynamics associated with the classical ebullition cycle no longer occur. Under highly subcooled conditions in low-g, it has been shown that for heater sizes where the primary bubble does not cause total dryout, bubble coalescence on the peripheral regions of the heater array causes similar heat transfer performance to classical 1-g nucleate boiling [10,11].

Studies on boiling in low-g indicate a strong gravitational dependence on CHF. Bubble coalescence has been observed to be the primary mechanism for CHF [10,11], which differs from the hydrodynamic instability model proposed by Zuber [12]. CHF in low-g was measured to be significantly smaller and occurred at lower wall superheats compared to higher gravity boiling. Kutateladze's model (Eq. (1)) inaccurately predicts the effect of gravity on CHF performance and could not correlate the data.

1.2. Thermocapillary flow

The absence of gravity increases the contribution of other mechanisms normally masked by natural convection and buoyancy, such as Marangoni or thermocapillary convection. Thermocapillary flow results from surface tension gradients along an interface which can form due to temperature gradients, material composition differences, and electrical potential variations or gradients [13]:

$$\frac{d\sigma}{dt} = \frac{\partial\sigma}{\partial T}\frac{\partial T}{\partial t} + \frac{\partial\sigma}{\partial c}\frac{\partial c}{\partial t} + \frac{\partial\sigma}{\partial\varphi}\frac{\partial\varphi}{\partial t} \quad (2)$$

Thermocapillary effects were observed by Trefethen [14] and McGrew [15] where it was shown that flow around vapor and air bubbles could be similar. They predicted that thermocapillary flow is the primary mechanism for boiling in low-g, replacing other boiling heat transfer mechanisms.

Strong surface tension driving flows have also been observed near an air bubble in silicon oil under applied temperature gradients [16]. Convective velocities near

the surface of a bubble on the order of 10^{-3} m/s were observed, which provided an additional force preventing departure in low-g.

Numerical studies performed on gas bubbles [17] showed that the magnitude of thermocapillary liquid flow is determined primarily by the Marangoni number (Ma),

$$Ma = \left|\frac{\partial\sigma}{\partial T}\right| \cdot \left|\frac{\partial T}{\partial t}\right| \frac{L^2}{a_1\eta_1} \tag{3}$$

the Prandtl number (Pr), and the Biot number (Bi). In addition, experimental results indicate that the flow may be very sensitive to surface active contaminants, a small amount of which can entirely suppress the thermocapillary motion. Most of the driving surface tension gradient was found to develop close to the liquid–vapor–solid interface and move even closer to the heater surface for higher Marangoni numbers. More recent studies have incorporated new interferometric techniques that allow the liquid motion and temperature gradients that exist during thermocapillary motion to be measured with greater accuracy [18].

Most of the above studies involve a binary system with either gas bubbles injected into the boiling chamber or large amounts of dissolved gases already present. For a gas bubble on a vapor surface, it is clear that temperature gradients can exist along the liquid–gas interface due to the lack of latent heat transport across the interface. For pure fluids however, much debate has centered on the ability of the bubble's liquid–vapor interface to maintain a temperature gradient during phase transition. Recent studies in low-gravity have indicated the formation of strong thermocapillary convection under highly subcooled conditions around a vapor bubble in systems with very low to minimal gas concentrations (nominally pure systems) e.g., [9–11]. It has been suggested by Straub [19] that thermocapillary flows can form in such systems in the following manner. In subcooled boiling, the top of a growing bubble may extend out of the superheated boundary layer and start to condense. With evaporation occurring near the three phase contact line, impurities such as dissolved gas are carried along with vapor to the top of the bubble. The vapor subsequently condenses while the non-condensable gases accumulate along the interface. Under steady-state conditions, the presence of the non-condensables reduces the vapor pressure locally along the interface thereby decreasing the saturation temperature locally. A negative temperature gradient oriented away from the heated surface and along the bubble interface forms, inducing thermocapillary motion from the base of the bubble to its top. This theory predicts an absence of thermocapillary motion under saturated conditions due to a nominally constant temperature interface.

1.3. Objectives

Previous work by the authors have indicated that thermocapillary convection has a strong role in determining heat transfer on small, square heaters $2.7 \times 2.7\ \text{mm}^2$ and smaller in low gravity environments [10,11]. The objective of this work was to obtain data on larger square heaters (up to $7 \times 7\ \text{mm}^2$) and on rectangular heated areas of various aspect ratio.

2. Experimental apparatus

2.1. Test rig description

An array of 96 platinum, serpentine resistance heater elements were deposited within a $7 \times 7\ \text{mm}^2$ area on a quartz wafer, and provided local surface heat flux and temperature measurements. The individual heaters were $0.7 \times 0.7\ \text{mm}^2$ in area, and had a nominal resistance of $260\ \Omega$ with a temperature coefficient of resistance of $0.0028\ ^\circ\text{C}^{-1}$. The lines that supply power to the heaters were routed between the heaters and a pin grid array ceramic package. Details of the construction of a similar heater array are given in [20]. Each heater in the array was kept at constant temperature by individual feedback circuits similar to those used in hotwire anemometry. The output of the circuit was the voltage across the heater, and the heat dissipated by a given heater could be calculated directly from this voltage and the heater resistance. The heater temperature was controlled by varying the wiper position of the digital potentiometer in one leg of the Wheatstone bridge. The frequency response of the circuit was measured to be 15 kHz. Additional details regarding the electronics of the circuits are given in [21]. When the individual heaters were quite a bit smaller than the bubble, the bubble saw, to a first approximation, a constant wall temperature boundary condition. On scales smaller than an individual heater, the boundary condition was neither constant wall temperature nor constant wall heat flux.

The test chamber was filled with nominally 3 l of FC-72. A bellows above the test chamber allowed the test section pressure to be changed when needed. A stirrer was used to break up any stratification within the test chamber before taking data, while a series of thin film heaters attached to the outside of the chamber were used to control the bulk liquid temperature. Video of the bubble motion was obtained through the heater (only 50% of the quartz substrate was covered by the heater lines) using a 30 Hz CCD camera. An air jet was used to cool the backside of the quartz wafer to ensure that all of the heaters were regulating.

2.2. Test procedure and data reduction

Data presented in this paper was taken aboard the NASA KC-135. During a portion of the parabolic flight, low-g levels (10^{-2} g) are produced. A typical flight consisted of 40 parabolic maneuvers. Each parabolic maneuver consisted of a high-g pullup (1.8 g), a low-g period of about 25 s, followed by a high-g pullout (1.6–1.7 g). Data acquisition for a particular wall temperature was initiated during the transition from high-g to low-g. Data were obtained for 90 s throughout the entire low-g period and into the high-g pullout and pullup. For a given flight, ΔT_{sub} was held constant while ΔT_{sat} was varied with successive parabolic maneuvers. Part of the heat supplied to the heater is dissipated into the substrate. Substrate conduction was subtracted from the heat input to obtain the heat transferred from the heater to the fluid. Time averaged data was taken in the low-g period where the heat transfer had reached steady state over an interval of 5–10 s. The reader is referred to previous papers [10,11] for additional details regarding the test rig and data reduction.

2.3. Degassing procedure

The air concentration in the liquid was reduced to less than 3 ppm by repeatedly pulling a vacuum on the vapor/air above the liquid. For a given partial pressure of gas (P_g) above the liquid, the dissolved gas concentration C_g (moles gas/mole liquid) in the liquid phase is given by Henry's law $C_g = H(T)P_g$ where $H(T)$ is Henry's constant. For air in FC-72, H has been measured to be 5.4×10^{-8} mole/mole Pa for 31 °C < T < 60 °C. P_g can be determined from a measurement of the total pressure (P_T) and temperature (T_{sat}) of the gas above the liquid after it has come to equilibrium in a sealed container from $P_g = P_T - P_{sat}(T_{sat})$ where P_{sat} is the saturation pressure of the liquid at the measured temperature T_{sat}. Consider now the case where liquid and air are sealed in a container of volume V, and that the volume of liquid containing dissolved air is V_l and the volume of vapor/air is V_g. We wish to determine the number of times V_g must be removed to reduce C_g below a specified value. The initial partial pressure of air above the liquid is assumed to be $P_{a,i}$. The initial concentration of gas in the liquid is then $C_{a,i} = H(T)P_{a,i}$. The mass of air in the liquid ($M_{a,l}$) can be shown to be:

$$M_{a,l} = H(T)P_{a,i}\rho_l V_l \frac{MW_a}{MW_l} \tag{4}$$

where MW_l and MW_a are the molecular weights of the liquid and air, respectively. If the vapor and air above the liquid are removed using a vacuum pump (we will assume the liquid volume does not change) and the chamber allowed to equilibrate, the air contained in the liquid must come out of solution to fill this volume. The total mass of air in the container is the sum of the air within and above the liquid:

$$H(T)P_{a,i}\rho_l V_l \frac{MW_a}{MW_l} = \frac{P_{a,i+1}}{R_a T} V_g + H(T)P_{a,i+1}\rho_l V_l \frac{MW_a}{MW_l} \tag{5}$$

where $P_{a,i+1}$ is the partial pressure of air above the liquid after the vacuum has been applied. Rearranging yields

$$\frac{P_{a,i+1}}{P_{a,i}} = \frac{H(T)\rho_l V_l \frac{MW_a}{MW_l}}{\frac{V_g}{R_a T} + H(T)\rho_l V_l \frac{MW_a}{MW_l}} = \frac{1}{1+Z} \tag{6}$$

where

$$Z = \frac{1}{R_a T H(T)\rho_l} \frac{V_g}{V_l} \frac{MW_l}{MW_a} \tag{7}$$

Eqs. (6) and (7) give the reduction in partial pressure of air above liquid due to the removal of the air and vapor above the liquid.

As an example, assume we wish to reduce the air concentration to below 3 ppm for liquid and air at 25 °C (this corresponds to a partial pressure of air of 55 Pa), and we have a container half filled with liquid ($V_g = V_l$). Using the properties of FC-72 ($MW_l = 0.34$ kg/mole, $\rho = 1680$ kg/m^3) and air ($MW_a = 0.028$ kg/m^3, $R_a = 286$ J/kg K), we find $Z = 1.57$, so the partial pressure of air is reduced to 39% of its previous value every time a vacuum is applied. If the initial total pressure is 101 kPa, then the vapor pressure is 36.6 kPa, and the partial pressure of air above the liquid is 64.7 kPa, resulting in an initial air concentration in the liquid of 3500 ppm. If we wish to reduce this to below 3 ppm, we find that a vacuum must be applied eight times.

Because the pressure in the chamber is never below the vapor pressure of the liquid, high performance vacuum pumps are not needed to thoroughly degas the liquid. In these measurements, the pressure was measured using a high-accuracy pressure transducer (PTG PX01C1-015A5T 15 PSIA, .01% FS). The accuracy of this transducer is about 10 Pa, well below the partial pressure of air at 3 ppm concentration. Accurate temperature measurements are also required. Near room temperature, the vapor pressure of FC-72 changes by about 1300 Pa/°C, so a 3 ppm error (55 Pa error) can result from a temperature change of 0.016 °C. The temperature was measured with a high precision RTD (Techne, Inc. model WSP350 PRT with TECAL Accutemp RTD indicator, ±0.001 °C). Both of our instruments were chosen such that the dissolved gas content could be determined to levels well below 3 ppm. In practice, the chamber pressure and temperature were measured just before degassing, and the pressure measurements were corrected to obtain what the total pressure would be at a reference temperature of 25 °C. A vacuum pump was then connected to the chamber and the pressure above the liquid was lowered long enough

to boil the liquid for a few seconds, ensuring that all of the vapor/air was removed. The pressure was observed to quickly stabilize to levels below what would be expected at $C_g = 3$ ppm after a few rounds. Once the liquid was degassed, the pressure around the bellows was brought up to 101 kPa—since there was no pressure differential across the seals in the boiling chamber, gas infiltration back into the liquid was minimized.

2.4. Uncertainty analysis

Uncertainties associated with the heater wall superheat, (ΔT_{sat}) are due to errors in the heater temperature resolution (2 digital potentiometer settings or 0.62 K), calibration temperature errors, and errors in the saturation temperature of the fluid which arise from uncertainties in the pressure measurement. Considering the worst case scenario, the saturation temperature of the fluid (T_{sat}) was calculated from a measurement of the time resolved pressure at the heater surface and the saturation curve data for FC-72. The pressure transducer was calibrated with an uncertainty of ±1.01 kPa. Incorporating this uncertainty into the saturation curve data, the resulting uncertainty in the time resolved saturation temperature is ±0.25 °C over the range tested. A propagation of uncertainty analysis of the heater wall temperature yields an error due primarily to the uncertainty in the temperature resolution of the heater, ±0.80 °C. The final uncertainty in the wall superheat is ±0.84 °C.

The thermistor used to measure the fluid temperature and the RTD used to the control the chamber sidewall temperature was calibrated in a constant temperature water bath using a NIST traceable liquid-in-glass thermometer. Although the thermistor measurement represents a local temperature value, it was assumed to be a representative average temperature of the bulk fluid. A micropump was used to minimize thermal gradients within the fluid between runs. For a given flight, the bulk temperature reading never varied by more than 2 °C. A summary of the test uncertainties is given in Table 1.

3. Results and discussion

Boiling curves for heaters of various aspect ratio along with videos of the bubble behavior were obtained in the low gravity environment provided by NASA's KC-135 in October, 2003. The heater aspect ratio was changed by varying the number of heaters powered (2×2, 2×4, 2×6, 2×8, 2×10, and 10×10) on a 7×7 mm^2 array. The bulk fluid was subcooled between 9 °C and 29 °C. This data is compared to previous data obtained using a 2.7×2.7 mm^2 array containing individual heaters 0.27×0.27 mm^2 in size (subcooling between 6 ° C and 31 °C).

Table 1
Summary of test uncertainties

Variable	Uncertainty (2σ)
Heat flux [W/cm^2]	±11.2%
T_h [°C]	±0.80 °C
T_{bulk} [°C]	±2.0 °C
T_{sat} [°C]	±0.25 °C
ΔT_{sat} [°C]	±0.84 °C
ΔT_{sub} [°C]	±2.02 °C
A_i [cm^2]	±5.0%

3.1. Subcooling effects on square heaters

Boiling curves for square heated areas of various size are shown in Fig. 1. Images of the boiling process are shown in Fig. 2a–c.

3.2. Low subcooling

Consider first the lowest subcooling cases ($\Delta T_{sub} = 6$ °C and $\Delta T_{sub} = 9$ °C). For the two smaller heater arrays (2.7 mm-6×6, and 2.7 mm-10×10), a large primary bubble forms over the heater surface and remains consistent in size over the wall superheat ranges tested (Fig. 2a and b). The primary bubble causes dryout over most of the powered heaters resulting in heat transfer levels less than 3 W/cm^2 for the superheats tested. Primary bubble departure did not occur during the approximately 20 s of low-g. For the largest heater (7 mm-10×10), the heat transfer increases with increasing superheat up to 26 °C, then decreases for a given subcooling. CHF for this heater is over 200% higher

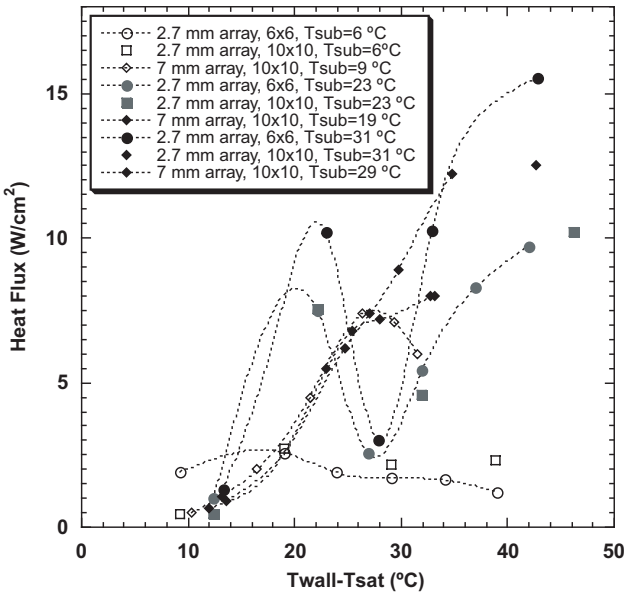

Fig. 1. Boiling curves on square heated areas of various size: 1.2×1.2 mm^2 (2.7 mm array-6×6 heaters), 2.7×2.7 mm^2 (2.7 mm array-10×10 heaters), and 7.0×7.0 mm^2 (7 mm array-10×10 heaters).

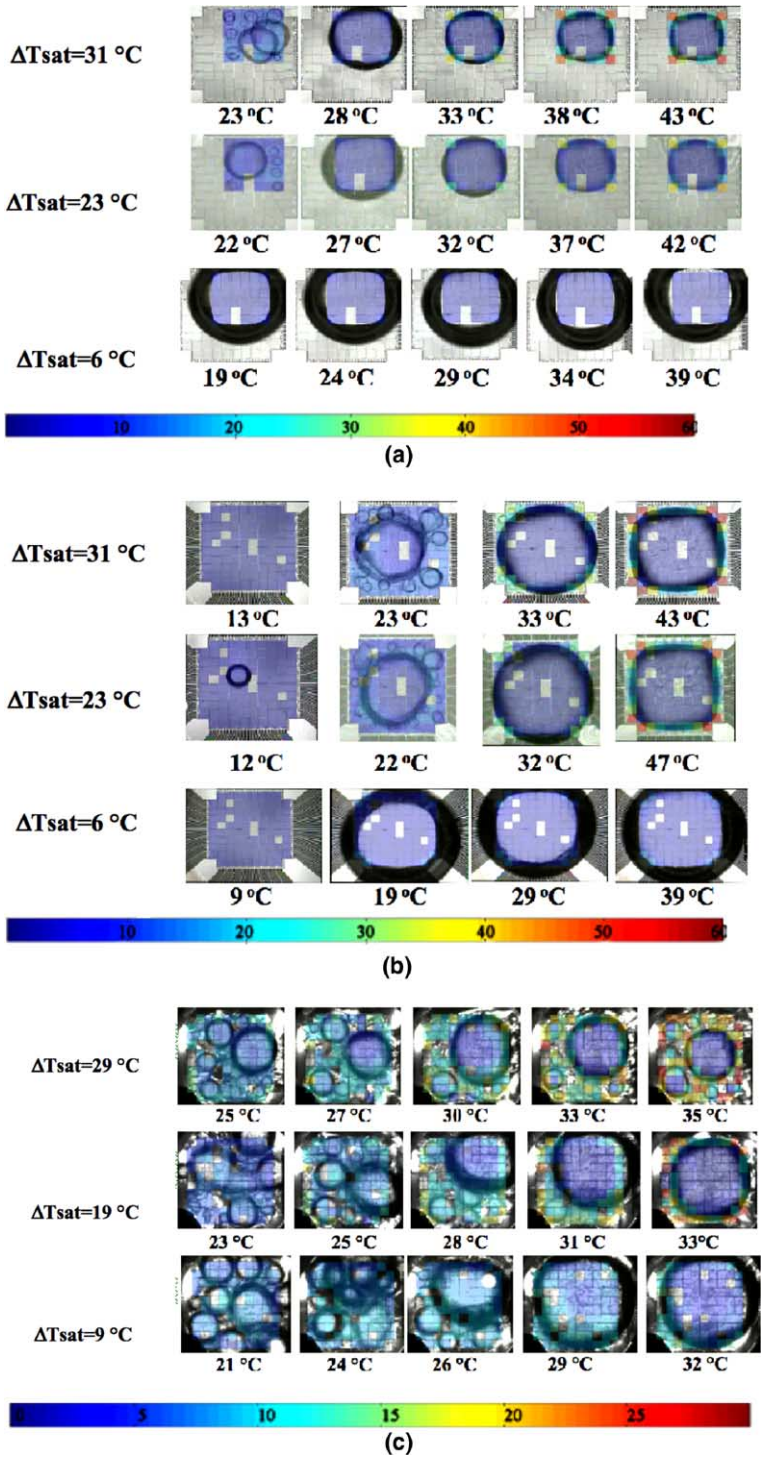

Fig. 2. Images of typical boiling behavior on square heated surfaces of various size. The superheat at which the images were obtained are listed below each image. Each heater in the array has been shaded according to the time average wall heat transfer [W/cm^2]. (a) 2.7 mm heater array, 6×6 array, (b) 2.7 mm heater, 10×10 array, and (c) 7 mm heater, 10×10 array.

than CHF for the two smaller heaters (Fig. 1). The reasons for this are apparent from the bubble dynamics (Fig. 2c). For the 7 mm heaters, the primary bubble increases in size as the superheat increases, but does not grow large enough to cover the entire heater. Occasional departure of the primary bubble also occurred, allowing the entire heated area to be rewet. Primary bubble departure in low-g may be due to induced liquid motion from the surrounding satellite bubbles and/or the significant g-jitter in all three axial directions aboard the KC-135. G-jitter has a much larger effect on the primary bubbles that form on the 7 mm array than on the smal-

ler heaters. Thermocapillary effects were not observed to be significant at this particular subcooling for all three heater sizes.

3.3. High subcooling

The heat flux at the highest subcooling (ΔT_{sub} = 29 °C and 31 °C) was much higher than for low subcooling. For the smallest heater (2.7 mm-6 × 6) in low-g, the boiling process was dominated by the primary bubble, which was significantly smaller than at low subcooling at a given superheat (Fig. 2a). At superheats lower than ΔT_{sat} = 23 °C (not shown), the primary bubble was significantly smaller than the heater size and few active nucleation sites were observed. The rapid increase in wall heat transfer as the superheat increases to 23 °C (CHF) was due to an increase in the number of active nucleation sites (the images shown in Fig. 2 are interlaced to convey the magnitude of bubble displacement). Coalescence with the primary bubble was observed to be the satellite bubble removal mechanism. As the superheat is increased to 28 °C, a sharp decrease in heat transfer occurs due to increased dry area on the heater. However, as the superheat was increased to 38 °C and above, increasingly stronger thermocapillary convection was observed, resulting in a decrease in the primary bubble size through an increase in the rate of condensation at the bubble cap. This allowed increased satellite bubble formation and an enhancement in heat transfer. As seen in Fig. 1, the heat flux at this superheat is 50% larger than at CHF. The trend in the boiling curve at this point indicates that a second local maximum heat flux may exist in low-g. Similar trends in the heat transfer data are observed for the ΔT_{sub} = 23 °C case, but the enhancement due to thermocapillary convection above ΔT_{sat} = 30 °C is not as significant.

Boiling curves for the 2.7 mm-10 × 10 array show trends similar to those for the 36 heater array. At high subcooling (ΔT_{sub} = 31 °C), the size of the primary bubble decreased resulting in an increase in satellite bubble formation. Coalescence was again observed to be the primary mechanism for CHF. Although strong thermocapillary convection was observed at high subcoolings and high superheats, data was not obtained with sufficient superheat resolution to determine whether a local maximum occurs after CHF, but the trends indicate similar behavior to that observed on the smallest heater. Heat fluxes up to 60 W/cm^2 were observed locally at the highest superheat.

Boiling on the 7 mm-10 × 10 array appeared to be again dominated by the characteristics of the primary bubble (Fig. 2c). At low superheats, the heat flux was much lower than on the smaller heaters, and may be due to a lack of nucleation sites on the larger heater array. At 25 °C superheat, visual observations of the boiling behavior appeared to be similar to those on the smallest heater, even though the smallest heater is in a transition boiling regime where thermocapillary effects are insignificant. As the superheat is increased to 30 °C, the primary bubble size reaches a maximum, but does not cause dryout on the heater. The heat flux continues to increase, however, due to a higher nucleation site density and heat transfer around the primary bubble. Further increases in superheat were accompanied by increases in thermocapillary convection which reduced the primary bubble size and increased the overall heat transfer. CHF was not reached since the satellite bubble heat transfer increased faster than the increase in the dry area fraction.

3.4. Intermediate subcooling

At the intermediate subcooling (ΔT_{sub} = 19 °C and 23 °C) the boiling is again dominated by the primary bubble. Trends similar to the high subcooling cases are observed in both the heat flux data and the images for all heater sizes.

3.5. Summary of heater size effects

In summary, low-g boiling behavior on square heaters appears to be governed by the dynamics of the primary bubble. Increased subcooling decreases the size of the primary bubble, allowing satellite bubbles to form with a corresponding increase in heat transfer. CHF appeared to be a result of the competition between increasing heat transfer associated with the satellite bubbles and the decrease in heat transfer due to growth of the dry area under the primary bubble as the wall superheat increases. Thermocapillary convection may be responsible for the post-CHF increase in heat flux observed on the two smaller heaters (2.7 mm-6 × 6 and 2.7 mm-10 × 10) at higher subcoolings. For the largest heater (7 mm-10 × 10), CHF was not observed.

Increased subcooling causes increased condensation at the bubble cap, resulting in a smaller bubble, which in turn increases the temperature gradient along the surface of the bubble. This leads to an increase in the strength of the thermocapillary convection, which brings cold liquid to the bubble cap increasing condensation, causing the bubble to shrink even further. The ultimate size of the primary bubble results from a balance between vapor removal by condensation and vapor addition by evaporation at the base and coalescence with the satellite bubbles.

3.6. Aspect ratio effects

Boiling curves for heaters of various aspect ratio (2 × 2, 2 × 4, 2 × 6, 2 × 8, and 2 × 10 heaters powered on the 7 mm array) at three subcoolings (9 °C, 19 °C, and 29 °C) are shown in Fig. 3. Images of the boiling

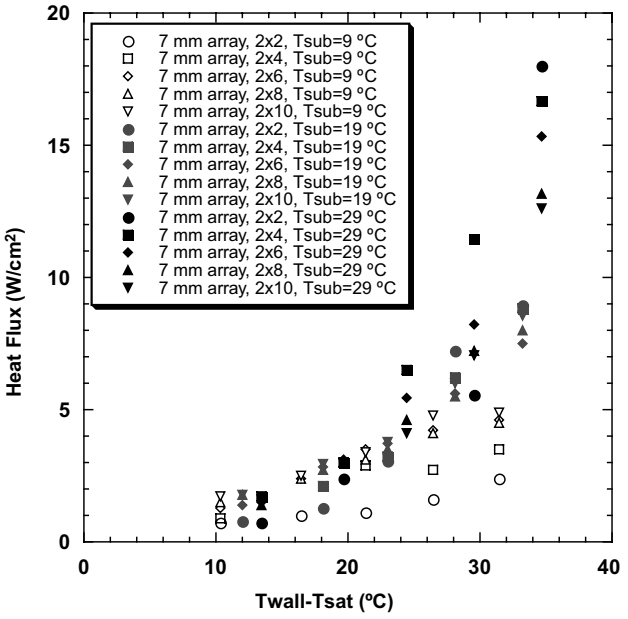

Fig. 3. Boiling curves on heaters of various aspect ratio.

behavior obtained through the heater array are shown in Fig. 4. In general, higher subcoolings for a given aspect ratio result in higher overall heat transfer. The boiling behavior at various subcoolings is described below.

3.7. Low subcooling

At low subcooling (ΔT_{sub} = 9 °C, red[1] symbols in Fig. 3), the heat flux appears to increase with increasing aspect ratio, especially at higher superheats. Thermocapillary motion around the bubble was quite weak. For example, at ΔT_{sat} = 31.4 °C (Fig. 4), it can be seen that large increases in the wetted area fraction occur as the aspect ratio increases from 2×2 to 2×6. On non-square heaters, surface tension acts to pull the bubble away from the ends of the array, allowing liquid to partially rewet the surface. Correspondingly larger increases in heat flux are observed. The wetted area fraction increases less dramatically between 2×6 and 2×8 with smaller increases in heat flux. On the 2×10 array, two large bubbles are observed, which may result in a nominally larger increase in wetted area and heat transfer. In the absence of thermocapillary effects, larger aspect ratio heaters may enhance the heater by allowing multiple bubbles to form on the surface.

3.8. High subcooling

At high subcooling (ΔT_{sub} = 29 °C, blue symbols in Fig. 3) the heat flux increases slightly with aspect ratio at low superheats (<20 °C). Visual observations indicated that the nucleation site density was very low. At higher superheats, the heat flux decreases as the aspect ratio increases, contrary to what was observed at low subcooling. At a superheat of ~24.6 °C, a single oblong bubble is observed on the 2×4 array (Fig. 4). Strong thermocapillary convection around the primary bubble was seen, as would be expected for high subcooling, causing it to shrink in size. This bubble was stationary on the surface as it merged with smaller bubbles nucleating at the ends of the array, accounting for the higher heat transfer at the ends. As the aspect ratio increases, the single bubble splits into two bubbles (2×6 and 2×8) due to surface tension effects. On the 2×10 heater, the increased heater area allows for additional nucleation sites, but similar heat transfer levels are observed. Heat fluxes up to 30 W/cm^2 are seen around the three phase bubble interface.

To a first approximation, the trends in the high subcooling data might be due to the increasing two dimensionality of the flow field around the heater. The 2×2 array experiences thermocapillary convection from all four sides of the array equally, causing the primary bubble size to shrink to its minimum value. As the aspect ratio increases, thermocapillary convection from the ends of the array become less important, and the bubble is cooled only on two sides.

3.9. Intermediate subcooling

At the intermediate subcooling (ΔT_{sub} = 19 °C), the data tends to collapse onto a single curve. This case represents a case where both thermocapillary convection and surface tension are important.

3.10. Summary

With varying aspect ratios, there appears to be two boiling mechanisms at play—thermocapillary convection and surface tension. In both cases, they result in increasing heat transfer when the wetted area increases. At low subcooling, it appears that the heat transfer increases due to an increase in wetted area fraction when surface tension acts to pull the bubble away from the heater edges at higher aspect ratios. At high subcooling, thermocapillary convection causes the primary bubble to shrink due to increased condensation, resulting in more wetted area.

3.11. Origin of thermocapillary convection

Strong thermocapillary convection was observed as the subcooling was increased. Its origins are not known. Previous researchers have observed that if the surface tension of water is lowered by as little as 0.1% due to contaminants, thermocapillary convection can be suppressed [17]. Other researchers [22–24] have observed

[1] For interpretation of the references in colour in figures, the reader is referred to the web version of this article.

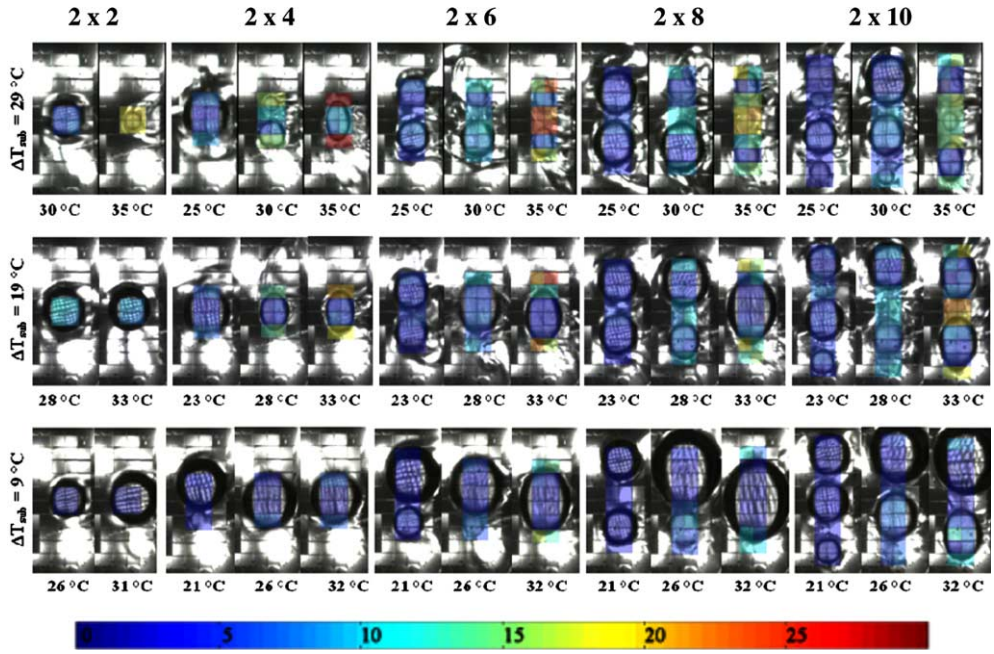

Fig. 4. Images of boiling on heaters of various aspect ratio. The superheat at which the images were obtained are listed below each image. Each heater in the array has been shaded according to the time average wall heat transfer [W/cm^2].

Table 2
Mass spectrometry study results on FC-72

Substance	MW	Composition based on GC peak area %	BP (°C)
n-Perfluorohexane	338	73.2	56
Perfluoro-2-methylpentane	338	17.892	57.66
Perfluoro-3-methylpentane	338	5.954	58.37
Perfluoro-2,3-dimethylbutane + perfluoro-2,2-dimethylbutane	338	1.723	
Perfluorocyclohexane	300	1.105	50.61
Perfluoromethylcyclopentane	300	0.126	48

strong thermocapillary convection in boiling of binary mixtures which delay the onset of CHF. We believe the thermocapillary motion observed in these experiments is not due to dissolved gas effects as suggested by Straub [19] since the gas concentration was reduced to well below 3 ppm. It may be due to contaminants in the system. Although reasonable care was taken to clean the system, it was not possible to remove all contaminants. Contaminants may have been introduced into the system from the O-rings used to seal the system, or the small amount of silicone RTV used to seal the PGA containing the heater array to the bottom of the test chamber. In addition, recent mass spectrometry studies aimed at determining the purity of FC-72 were performed. FC-72 was found to consist of a number of compounds at relatively high concentrations as shown in Table 2. Although significant quantities of perfluoro-2-methylpentane and perfluoro-3-methylpentane were measured, their boiling temperatures are similar to that for *n*-perfluorohexane. Perfluorocyclohexane and perfluoromethylcyclopentane were present in smaller concentrations, but their boiling points are significantly different from that of *n*-perfluorohexane, and may be the cause of the strong thermocapillary convection observed in this study. These substances may accumulate at the top of a stable primary bubble in low-g, reducing the saturation pressure locally and causing a temperature gradient to form along the bubble interface. Additional analysis is required to ascertain the full effects of these substances.

4. Conclusions

Low-g boiling behavior is governed by the dynamics of the primary bubble. For both square and rectangular heaters, CHF appears to be a result of the competition between increasing heat transfer associated with the satellite bubbles and the decrease in heat transfer due to growth of the dry area under the primary bubble as

the wall superheat increases. At low superheats on rectangular heaters, surface tension acts to pull the bubble away from the heater ends, allowing liquid to re-wet the surface. At high superheats, thermocapillary convection causes the large bubbles that form on the surface to shrink by increasing the condensation on the bubble cap, resulting in more wetted area.

Acknowledgments

This work was supported by the Office of Biological and Physical Research at NASA Headquarters, Grant No. NCC3-783. The grant monitor is Mr. John McQuillen.

References

[1] R. Viskanta et al., Microgravity research in support of technologies for the human exploration and development of space and planetary bodies, Topical Report of the National Research Council, Space Studies Board, 2000.
[2] P. DiMarco, Review of reduced gravity boiling heat transfer: European Research, Japan Society of Microgravity Application Journal 20 (4) (2003) 252–263.
[3] J. Kim, Review of reduced gravity boiling heat transfer: US Research, Japan Society of Microgravity Application Journal 20 (4) (2003) 264–271.
[4] H. Ohta, Review of reduced gravity boiling heat transfer: Japanese Research, Japan Society of Microgravity Application Journal 20 (4) (2003) 272–285.
[5] F.C. Gunther, F. Kreith, Photographic study of bubble formation in heat transfer to subcooled water, Prog. Rept. 4-120, Jet Propulsion Lab., California Institute of Technology, Pasadena, CA, March, 1956.
[6] H.K. Forster, R. Greif, Heat transfer to a boiling liquid—mechanisms and correlations, Journal of Heat Transfer 81 (1959) 45.
[7] S.S. Kutateladze, Heat transfer during condensation and boiling, translated from a publication of the State Scientific and Technical Publishers of Literature and Machinery, Moscow-Leningrad, as AEC-TR-3770, 1962.
[8] H.J. Ivey, D.J. Morris, On the relevance of the vapor–liquid exchange mechanism for subcooled boiling heat transfer at high pressure, British Rep. AEEW-R-137, Atomic Energy Establishment, Winfrith, 1962.
[9] H. Merte, H.S. Lee, R.B. Keller, Dryout and rewetting in the pool boiling experiment flown on STS-72 (PBE-IIB) and STS-77 (PBE-IIA), NASA Report #E-11185, 1998.
[10] J. Kim, J.F. Benton, Subcooled pool boiling heat transfer at various gravity levels, International Journal of Heat and Fluid Flow 23 (4) (2002) 497–508.
[11] J. Kim, J.F. Benton, D. Wisniewski, Pool boiling heat transfer on small heaters: effect of gravity and subcooling, International Journal of Heat and Mass Transfer 45 (19) (2002) 3921–3934.
[12] N. Zuber, On the stability of boiling heat transfer, Transactions of the ASME 80 (1958) 711–720.
[13] S. Ostrach, Natural convection heat transfer in cavities and cells, in: Proceedings of the 7th International Heat Transfer Conference, vol. 1, 1982, pp. 365–379.
[14] L. Trefethen, On the jet propulsion of bubbles in a heater liquid, Tufts University Mechanical Engineering Rep., 61-8-1, 1961.
[15] J.L. McGrew, T.R. Bamford, Marangoni flow: an additional mechanism in boiling heat transfer, Science 153 (3740) (1966) 1106–1107.
[16] D. Raake, J. Siekmann, Temperature and velocity fields due to surface tension driven flow, Experiments in Fluids 7 (1989) 164–172.
[17] Y.S. Kao, D.B.R. Kenning, Thermocapillary flow near a hemispherical bubble on a heater wall, Journal of Fluid Mechanics 53 (1972) 715–735.
[18] Y. Abe, A. Iwasaki, Single and dual vapor bubble experiments in microgravity, in: Proceeding of the Microgravity Fluid Physics and Heat Transfer Conference, September 19–24, Kahuku, Hawaii, 1999.
[19] J. Straub, Origin and effect of thermocapillary convection in subcooled boiling: observations and conclusions from experiments performed at microgravity, Annals of the New York Academy of Sciences 974 (2002) 348–363.
[20] T.D. Rule, J. Kim, Heat transfer behavior on small horizontal heaters during pool boiling of FC-72, Journal of Heat Transfer 121 (2) (1999) 386–393.
[21] S. Bae, M. Kim, J. Kim, Improved technique to measure time- and space-resolved heat transfer under single bubbles during saturated pool boiling of FC-72, Experimental Heat Transfer 12 (3) (1999) 265–278.
[22] S. Ahmed, V.P. Carey, Effects of gravity on the boiling of binary fluid mixtures, International Journal of Heat and Mass Transfer 41 (16) (1998) 2469–2483.
[23] Y. Abe, T. Oka, M.H. Mori, A. Nagashima, Pool boiling of non-azeotropic binary mixture under microgravity, International Journal of Heat and Mass Transfer 37 (1994) 2405–2414.
[24] C.I. Sun, V.P. Carey, Effects of gap geometry and gravity on boiling around a constrained bubble in 2-propanol/water mixtures, in: Proceedings of the 2003 ASME Summer Heat Transfer Conference, Las Vegas, 2003.